

Sweepback Effects on the Lift, Drag, and Pitching Moment Coefficients for a B-1 Bomber Model in a Subsonic Speed Regime

K. Koirala¹, C. Kong², U. Tran³, J. Villavicencio⁴
Wichita State University, Wichita, Kansas 67260-0044

The introduction of the variable swept wing design provided the capability of changing an aircraft's planform in flight. Unswept wings were generally used for lower speed flights, while swept wings provided flight capabilities in higher speed regimes; hence, changing the sweep settings allowed the aircraft to optimize for different mission requirements. Unfortunately, accurate predictions for the aerodynamic characteristics for an aircraft with a variable swept wing design, such as the B-1 Bomber, is difficult. As a result, acquiring data from wind tunnel tests is critical to accurately determine the optimal angle of attack and corresponding sweep angle settings in order to maximize C_L and minimize C_D on the B-1 Bomber; this becomes the overall objective of this experiment.

Nomenclature³

AOA	=	angle of attack
C_L	=	aircraft lift coefficient
C_D	=	aircraft drag coefficient
C_M	=	aircraft pitching moment coefficient
CG	=	center of gravity
q	=	dynamic pressure
WSU	=	Wichita State University

I. Results Summary¹

Experimental analysis of a 1:48 scaled B-1 Bomber model is presented in this report. The model was tested at 5 different sweep angles as measured to the leading edge of the wing: 21°, 32°, 43°, 54° and 65°. In addition, alpha-sweeps from -8° to 16° were considered, where data was acquired in 4° increments. Aerodynamics forces and moments were recorded using the data acquisition software in WSU's 3' X 4' wind tunnel.

The analytical results from testing demonstrated that sweeping the wing back will reduce the drag, though a compromise must be made with the lift generated. Pitching moments varied significantly as the aircraft center of pressure translated aft when the sweep is increased; this limits the alpha-sweep conducted, since the pitching moment limits of the wind tunnel is a constraint that must be considered. The performance of the model (i.e., the lift-to-drag ratio) did decrease with increasing sweep angles, as predicted.

The model was tested at 0.14 Mach; hence, the flow can be assumed to be steady, incompressible and irrotational. The B-1 Bomber aircraft operates under much higher Reynolds Number in comparison to the Reynolds number for the B-1 model when operated in the wind tunnel. However, the results obtained are useful in terms of predicting the performance of a variable swept wing aircraft within the subsonic regime.

¹ Student, Aerospace Engineering, AIAA Student member.

² Student, Aerospace Engineering, Non-member.

³ Student, Aerospace Engineering, AIAA student member.

⁴ Student, Aerospace Engineering, Non-member.

A. Model Specifications

Utilizing a B-1 Bomber model for testing purposes was decided on since it incorporated a variable swept wing design, and because it was readily available at WSU. Prior to testing in the wind tunnel, dimensions from the model were recorded for calculation purposes, and to ensure that the model was indeed was a 1:48 scale of the actual aircraft. Results from these measurements are presented alongside the actual aircraft specifications in Table 1.

Table 1: Specifications for the B-1 Aircraft and B-1 Model

Characteristics	Real Aircraft (Ref. 1)		Model	
Length	147 ft		36.75 in	
Wingspan	Extended	136.7 ft	Extended	34.175 in
	Swept	78.2 ft	Swept	19.55 in
Sweep Angle	Fully Extended	15°	Fully Extended	21°
	Fully Swept	65°	Fully Swept	65°
Height	34 ft		2 in.*	
Weight	Empty	192,133 lb	12 lb	
	Max. Takeoff	477,000 lb		
Max. Speed	825 mph		110 mph	

*Height was considered without landing gear height since this component was not included with the model.

B. Model Repair

After confirming the model was 1:48 scale, repairing the model became a priority for safety reasons, and to obtain accurate wind tunnel results. Initial signs of disrepair included chipped edges on the empennage and wing surfaces, a missing nozzle on an engine which had become detached from the model, open holes, and dented surfaces on the model. Bondo was used to fill the open holes, to build dented areas, to reconstruct the missing nozzle, and to fix the chipped edges on the empennage and wing. The bondo was allowed to cure for at least 24 hours before it was sanded down into a smooth surface.

Once this was completed, the model was painted with two coats of paint. The first coat acts as a protective layer on the model, while the second coating ensures a smooth surface.

C. Securing Sweep Angles

To secure the wing sweep angle during testing, two solutions were considered. The first solution consisted of securing the wing with aluminum tape at the wing root chord. Unfortunately, after testing this solution, the aluminum tape was found unable to sustain the shear stresses when minimal force was applied at the wing tip.

The second solution consisted of securing the wing by pinching the wing, whereby a screw is secured near the pivot point locations on the wing. When a force is applied at the wing tip, the screw also failed to secure the wing. Since the flat surface near the pivot point was resting against the flat end of the screw, an insufficient friction force was present; this force proved unable to stop the wing from rotating. As a result, electrical tape was attached to the

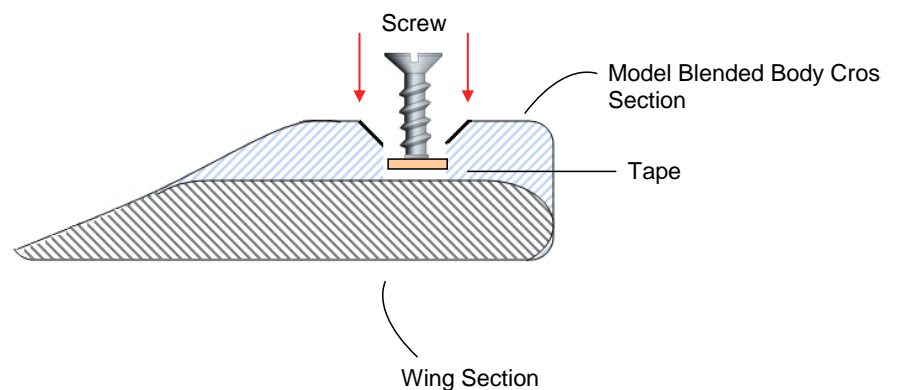


Fig. 1: Securing Mechanism – Cross-Section View. When the desired sweep angle is positioned, a screw with electrical tape attached to the end will be fastened to the model. The tape creates additional friction which arrests the wing's movement.

end of the screw and adhered to the flat surface of the pivot point, thus securing the sweep angle (see Fig. 1). When a force is applied on the wing tip, the wing remains rigid, and maintains a constant sweep angle.

Concurrently during this time, the desired sweep angles were marked on the wing's surface (see Image 1). A difference was noticed between the wing fully extended sweep angle on the B-1 aircraft, and the model's sweep angle with fully extended wings. The aircraft has a fully extended wing with 15° of sweep built into the design, whereas the model contains 21° of sweep when the wing is fully extended. Hence, testing the model's sweep angles was limited to an initial sweep angle of 21° with testing being completed in 11° increments to the fully swept wing angle of 65° .

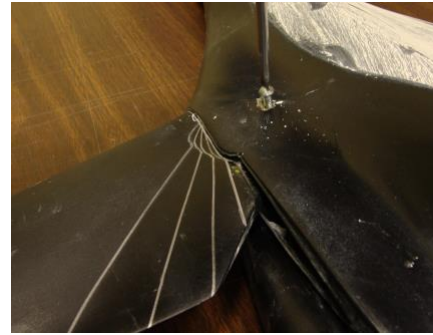


Image 1: Desired swept angle and securing location.

D. Construction of the Mounting Plate

The mounting plate was constructed to meet the dimensions of the mounting plane of the wind tunnel balance system (see Fig. 2). The mounting plate was secured at two existing screw holes located on the bottom surface of the model as shown in images 2 and 3. The mount was constructed such that the balance reference center would remain as close as possible to the CG of the model. Image 3 shows how the model was mounted to the balance system with only 4 screws; the middle 2 screws and the 2 aft-most screws. Upon mounting the model in the tunnel, it was discovered that the fore-most 2 screws would contact the balance at higher angles of attack, causing part of the load to be transferred to balance system.

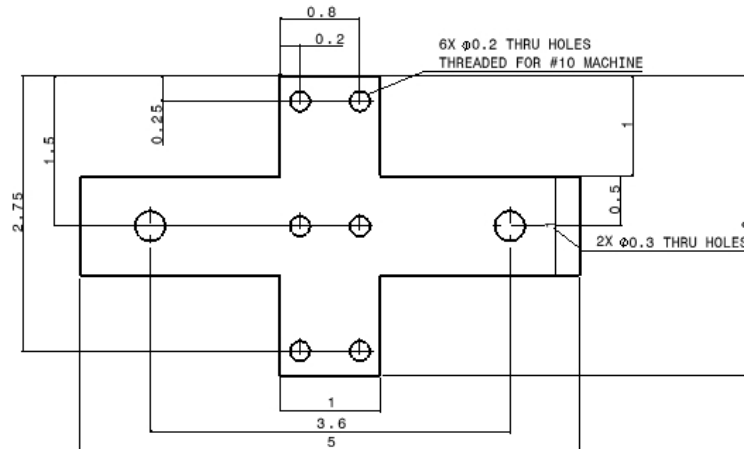


Fig. 2: CATIA drawing of mounting plate specifications. All measurements are shown in inches.



Image 2: Marked location for securing mounting plate.



Image 3: Secured mounting plate on the model.

II. Test Matrix⁴

A total of 35 runs including dynamic tares, static tare, flow visualization, and runs with and without flow trips were completed. Three dynamic pressures were considered for testing: 20 psf, 25 psf, and 30 psf. Unfortunately, during the day of the test, maximum q achievable was 29 psf, hence, 29 psf is used in place of 30 psf. Each set of runs is comprised of testing a sweep angle at these three dynamic pressure values (see Table 2).

After completing the first set of runs, a repeat run was conducted to ensure the results obtained from the data acquisition software were consistent. Comparing the results from this repeat run with the initial run indicated the largest difference to be 0.054 between the dynamic pressure values.

To prepare for runs with flow trips on the model, strips of aluminum tape were cut using pinking shears to create serrated edges on the tape. This allows the tape to energize the airflow as it passes the tape. The tape was then attached to the nose, and on the upper and lower surfaces of the wing and tail leading edge areas. Test runs conducted with flow trips were carried out at maximum dynamic pressure (29psf). A total of 5 flow trips runs were made, one for each sweep angle, and with an alpha-sweep from -8° to $+16^\circ$.

Following the completion of the flow trip runs were the flow visualization runs. For flow visualization, a china clay and kerosene mixture were brushed over the surface of the model. It is important to remember that once the china clay-kerosene mixture is brushed on the model surface, it dries very quickly, hence, having the model in the desired configuration and at the desired AOA is essential. Seven flow visualization runs were completed: two for 65° sweep angle with flow trips at AOAs of 0° and $+16^\circ$; two flow trip runs for 21° sweep angle without flow trips and at AOAs of 0° and $+16^\circ$, and lastly, three runs at 65° sweep angle without flow trips and at AOAs of 0° , -8° and $+16^\circ$.

Table 2: Summarized Test Matrix of the sets of test runs completed in the 3'x4' wind tunnel.

Run Set	Sweep Angle(β)	A sweep*	q (psf)
Dynamic Tare	-	-8° to $+16^\circ$	20, 25, 29
Static Tare	Fully Extended(21°)	-8° to $+16^\circ$	-
1	Fully Extended(21°)	-8° to $+16^\circ$	20, 25, 29
Static Tare	32°	-8° to $+16^\circ$	-
2	32°	-8° to $+16^\circ$	20, 25, 29
Static Tare	43°	-8° to $+16^\circ$	-
3	43°	-8° to $+16^\circ$	20, 25, 29
Static Tare	54°	-8° to $+16^\circ$	-
4	54°	-8° to $+16^\circ$	20, 25, 29
Static Tare	Fully Swept (65°)	-8° to $+16^\circ$	-
5	Fully Swept (65°)	-8° to $+16^\circ$	20, 25, 29
Flow Trip	21° , 32° , 43° , 54° , 65°	-8° to $+16^\circ$	Maximum
Flow Trip	Fully Swept (65°)	-8° to $+16^\circ$	Maximum
Flow Visualization (w/ Flow Trips)	Fully Swept(65°)	0°	30
Flow Visualization (w/o Flow Trips)	Fully Swept(65°)	0° , $+16^\circ$	Maximum
Flow Visualization (w/o Flow Trips)	Fully Extended(21°)	-8° , 0° , $+16^\circ$	Maximum

III. Predicted Results and Test Results³

E. Predicted Results

Initial predictions for the lift were undertaken to ensure that the wind tunnel lift load limit of 35 lbs was not exceeded. To predict the lift values of the model, the lift was calculated utilizing airfoil data from *Theory of Wing Sections*. Two airfoils were chosen: one for the wing-body, and one for the horizontal tail. Since the horizontal tail of the model closely resembled a flat plate, the symmetrical airfoil NACA 0006 was utilized to predict the lift contribution from the horizontal tail (Ref. 2).

When calculating lift for the wing-body, the area of the fuselage is included in the wing area. In this way, the lift contribution from the fuselage can also be considered. Data from the NACA 4412 airfoil was utilized to predict the lift contribution from the wing-body. Prediction results are shown in Fig. 3 (Ref 3).

Observe how the lift generated at a dynamic pressure of 30 psf does exceed 35 lbs of lift. However, this was not seen as a major source of concern since the airfoil data was extrapolated at a Reynolds number of 300,000, whereas the Reynolds number for the model is closer to 80,000 indicating the test results for the lift force generated would be much lower than predicted. Hence, unless the lift generated was much larger than 35 lbs, such as lift values exceeding 45 lbs, predictions indicate the lift generated will not exceed wind tunnels lift load limit. Results from testing confirmed the lift load limit was not exceeded (see G. Test Results).

Predicted Lift Polar for Various Q Values

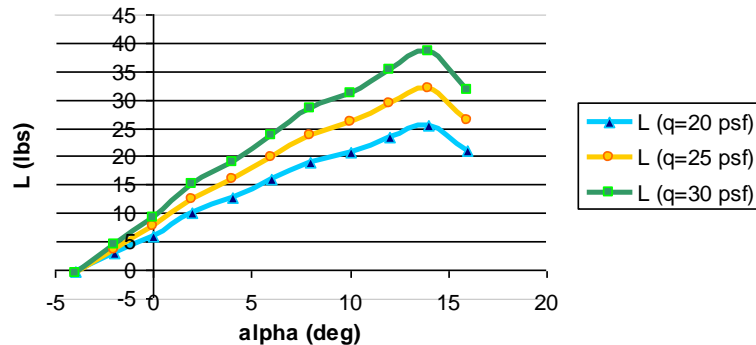


Fig. 3: Predicted lift behavior as a function of Angle of Attack.

F. Variation of Predicted Results with Sweep Angle

Since the B-1 has a complex fuselage geometry, and additional components such as the engines and sensors, accurate predictions for the variation of lift, drag, and pitching moment with different sweep angles would have been difficult to model. Instead, the relative trend of lift and drag behaviors as the sweep angle is increased was researched.

Anderson states that “for subsonic flight, increasing the wing sweep reduces the lift” (Ref. 4) Hence, the curves in Fig. 3 are expected to translate further such that lift values will be closer to the abscissa as the sweep angle is increased. This was validated during testing and can be seen in the lift polar provided in Fig. 6.

Anderson also presents the variation of the lift-to-drag ratio with sweep angle shown in Fig. 4. One can observe how the lift-to-drag ratio decreases dramatically as the sweep angle is increased from 40° to 60° sweep. Since the B-1 model has a maximum sweep of 65°, only values from 20° to 65° were extrapolated from Anderson and compared to the test results.

General behaviors for drag and pitching moment could not be found during the research; hence testing results were analyzed without prior predictions.

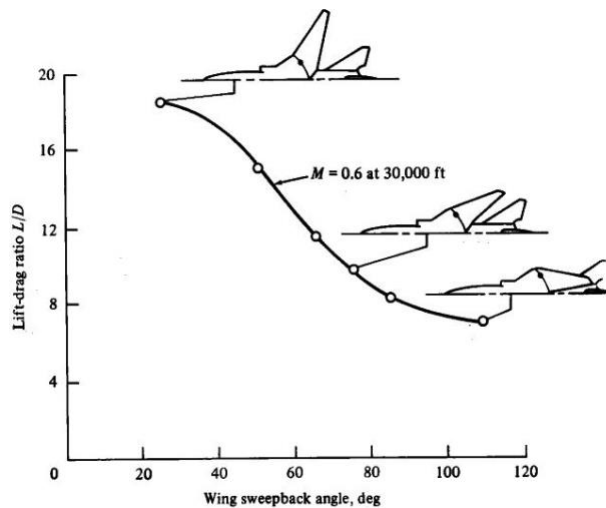


Fig. 4: Variation of lift-to-drag ratio with sweep angle as presented by Anderson (Ref. 4).

G. Test Results

When a comparison is made between the results that Anderson presents and the collected data from the experiment, one can see how the trend of the curves are close, signifying the concurrence of the test results with historical results (see Fig. 5). In addition, one will notice how the test result curves are translated a great distance from Anderson's results. This is due to the speed differences under which Anderson's tests were conducted as compared to the speed under which this experiment was operating under. From Fig. 4, comments within the figure indicate the test was conducted at 0.6 Mach. In comparison, for a maximum q value of 29 psf, the maximum speed found in this experiment was 0.14 Mach, a significant difference.

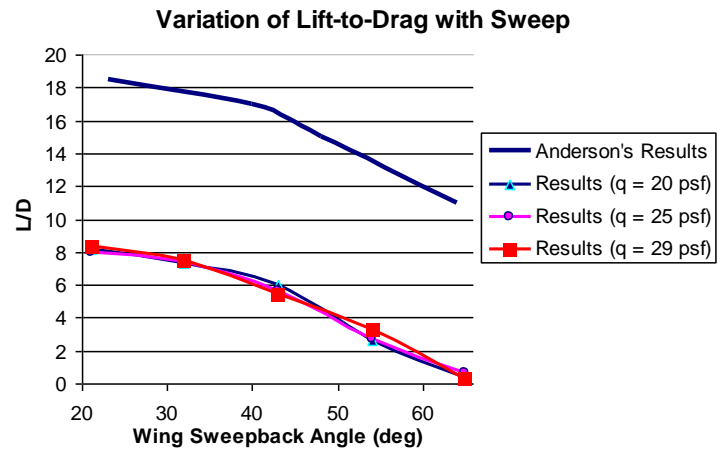


Fig. 5: Comparison of test results with Anderson's results for the variation of the lift-to-drag ratio with sweep angle.

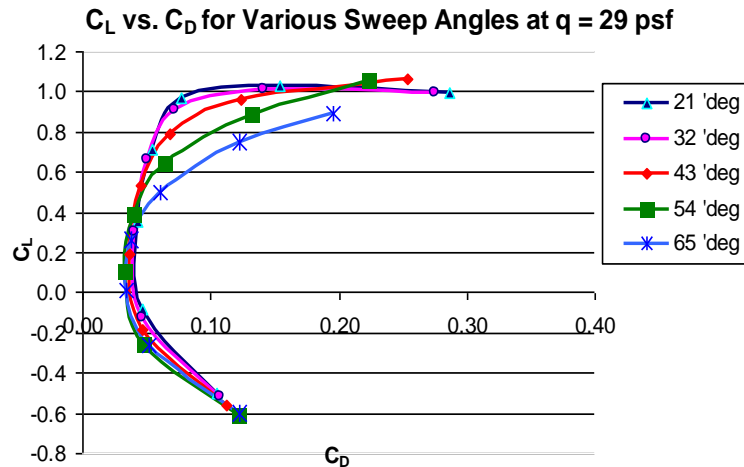


Fig. 6: Comparison of C_L values for each C_D value found for each sweep angle tested.

When the results are reduced into C_L and C_D data, and plotted, the observation can be made that greater sweep angles result in lower values of C_L for each C_D considered. Recall the objective of this experiment was to determine the optimal angle of attack and corresponding sweep angle settings to maximize C_L and minimize C_D on the B-1 Bomber within a subsonic speed regime. From Figure 6, the results indicate the optimal setting to achieve maximum C_L values for minimal C_D values would include utilizing a wing which incorporates 21° of sweep as measured to the wing leading edge. To determine what the optimal angle of attack would be, a plot of the lift polar for the various sweep angles was plotted (see Fig. 7). From Figure 7, one can observe the aircraft is approaching stall at an AOA of 8° when 21° of sweep is considered. Hence, the optimal angle of attack would be 8° .

After considering the lift and drag behavior of the model in test results, the pitching moment was analyzed. Figure 8 demonstrates how increasing the sweep angle causes the pitching moment to increase. This is logical, since sweeping the wing back shifts the aircraft center of pressure further aft. An interesting phenomenon can be seen when comparing Figure 7 & 8 concurrently. Notice how at higher sweep angles (e.g., 54° and 65° sweep) the slope of the pitching moment polar becomes positive, indicating the approach of stall, however the lift curves for these higher angles of sweep remains

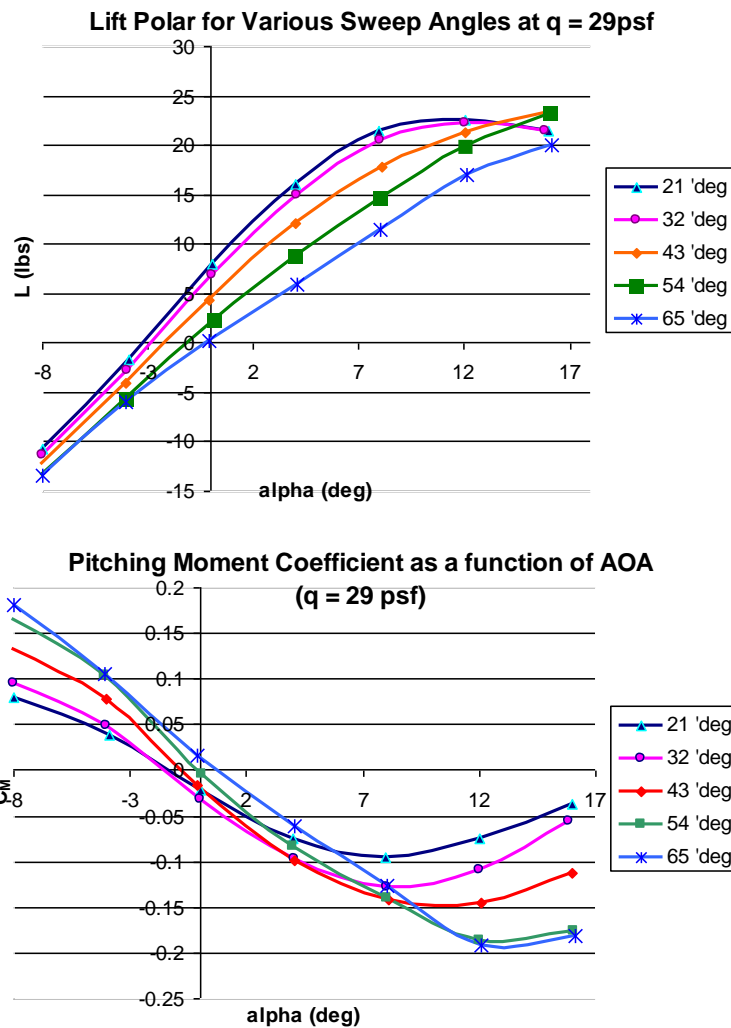


Fig. 8: Pitching moment coefficient is considered about the calculated aerodynamic center for the model.

linear during this time. Flow visualization images explain these increases in lift as being the result of vortex induced lift (see **IV. Flow Visualization** for more details.)

H. Correction Factors and Standard Deviations

To correctly interpret the results from wind tunnel tests, several correction factors must be made. These corrections include removing static and dynamic tare effects, translating the pitching moment from the balance system's reference center to the calculated aerodynamic center, and accounting for the model's solid blocking effects.

Calculation of the model aerodynamic center was undergone with the following assumptions: the distance between the model reference center and the actual aerodynamic center location along the z-axis is small, hence any corrections along the z-axis is neglected (see Fig. 9).

Solid blocking corrections were included in the data analysis process using Thom's solid blocking correction equation (Ref. 5).

In addition to these corrections, standard deviations for lift, drag and pitching moment were given through the data acquisition software. During the analysis of the data, it was noticed that the standard deviation for the lift, drag, and pitching moments at different dynamic pressure values varied significantly, on the other hand, the standard deviation for these same aerodynamic characteristics for test runs completed at the same dynamic pressure, but at different sweep angles resulted in standard deviations that were consistently close in value, thus indicates the standard deviation is mostly independent of the configuration tested. Table 3 summarizes the average standard deviation for test runs completed.

Table 3: Standard Deviations averaged over sets of test runs operating at similar q values.

q (psf)	L_{stdev} (lb)	D_{stdev} (lb)	PM_{stdev} (ft.lb)
20	0.987	1.022	-1.033
25	1.626	1.358	-1.343
29	2.154	1.531	-1.509

IV. Additional Test Runs

I. Flow Trips¹

Flow tripping is a method utilized to simulate flight conditions during slow speed wind-tunnel testing. Aluminum tape was serrated and then attached to the leading edges of the wing, tails, and the nose to trip the flow. The model was then tested at the maximum ' q ' possible. Flow visualizations were also completed using the flow trips to observe effects on the boundary layer. Image 10 shows the effects of tripping the flow, on the boundary layer. As a result of flow tripping, one can observe the $C_{L_{\text{max}}}$ has increased compared to the $C_{L_{\text{max}}}$ values for test runs without trips, though there is also a significant increase in the C_D (see Fig. 10 & 11). At a sweep of 54° the model did not stall during the flow trip run even when the model was inclined at 16° AOA. Flow visualizations showed that there were vortices being generated on the leading edge of the wings resulting in vortex-lift being generated, which explains the delay in the stall.

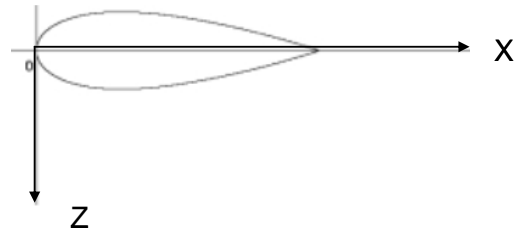
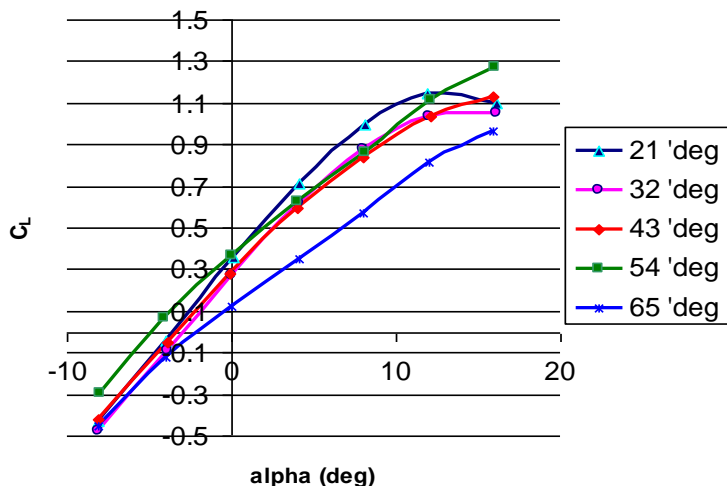


Fig. 9: Reference axis considered at the leading edge of the wing root chord for aerodynamic center calculations.



Image 4: Attached turbulent flow for tripped flow.
Configuration: Angle of attack of 16° ,
Dynamic Pressure of 29 psf

**Variation of Lift Coefficient with Angle of Attack
With Flow Trips ($q = 29$ psf)**



**Variation of Lift Coefficient with Angle of Attack w/o
Flow Trips ($q = 29$ psf)**

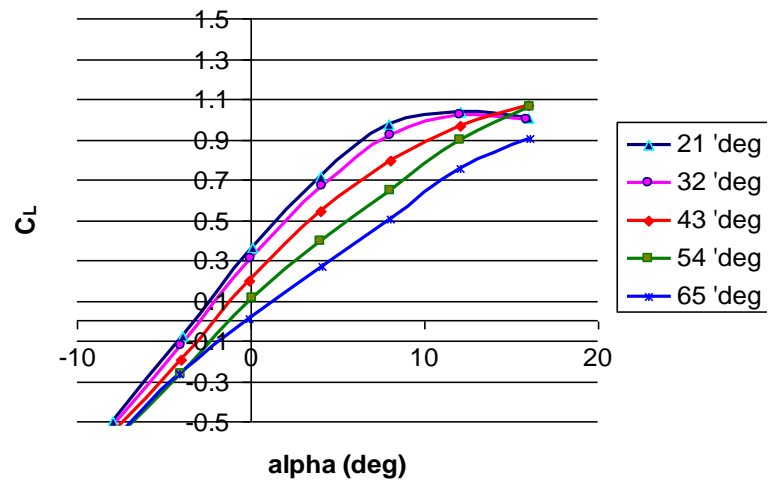


Fig. 10 & 11: Comparison between Lift Polar Curves for Runs with and without Flow Trips. The attached turbulent layer for runs with flow trips causes a greater lift production. Hence, in actual flight conditions the lift generated would be greater than the values obtained in the wind tunnel for runs without flow trips.

J. FlowVisualization²

China clay and kerosene were used for the visualization test. Since the china clay and kerosene compound dries quickly, only half of the model is coated. Coating the model required brushing the compound on in a crosswise motion perpendicular to the air flow, thus allowing one to differentiate between brush strokes that have dried in the coating with the air flow effects over the model.

Due to time constraints, select visualization tests were conducted, all of them at maximum dynamic pressure of 29 psf. See Table 4 & 5 for flow visualization results.

Table 4: Flow Visualization for Wing Fully Extended (21°)







Fully Extended (21°)		
Results	AoA	Description
	0°	Nice and steady air flow along the entire model body at this AoA compared to 16° AoA.
	0°	The Transition between laminar and turbulent boundary layer can be clearly seen on the picture. The separation on the flow is due to lack of energy. Flow tripping would attach the turbulent boundary layer to the surface for much longer.
	16°	Flow separation and reverse flow can be seen on the model surface at higher angle of attacks, which results in huge drag increment and stall on the model.

Table 5: Flow Visualization for Wing Fully Extended (21°)

Fully Swept (65°)		
Results	AoA	Description
	16°	Formation of vortices began from the bottom of the nose at high AoA.
	0°	Larger laminar flow on the wing at fully swept angle (65°) compared to the fully extended angle (21°). This also caused reduction in significant amount of drag.
	16°	Leading edge vortices have formed, compare this to the flow separation observed when the wing is fully extended at high AoA. The horizontal tail shows flow reversal effects. At this configuration the model hasn't stalled though the tail shows signs of stall because of the induced vortex lift.

V. Concluding Remarks¹

To quickly summarize the results, the reduction of data obtained from wind tunnel test indicated that increasing the sweep angle back significantly reduced the drag, making this configuration optimal for higher speeds, whereas the increased lift production of a fully extended wing is recommended for takeoffs and cruise at subsonic speeds.

The pitching moment increases rapidly as the wings are swept back because the center of pressure of the aircraft moves further aft. If only takeoff and cruise is considered within the subsonic speed regime, the fully extended wing is recommended to deter the increase in pitching moments.

Should further testing be implemented based on the results of this experiment, several suggestions are presented on possible further studies that could be conducted:

- 1) Repeat the experiment at higher speeds to obtain the effects of variable sweep on drag divergence Mach number. In this experiment, the Lift/Drag ratio decreased as the sweep angle increased, however, at higher speeds ($M=0.6+$) the drag divergence Mach Number increases proportionally to the square of the sweep angle. (Ref. 6)
- 2) Reconstruction of the model to incorporate airfoil cross-sections to increase the probability of accurate predictions on flow behavior and the aerodynamic behavior of the aircraft.
- 3) Use of the subsonic data acquired in this experiment to extrapolate supersonic results considering compressible flow and performing numerical analysis.
- 4) Analysis of the wing-body interferences.

References³

- 1) North American Aircraft Rockwell International, "B-1B FACTBOOK," Rept. NA 95-1210.
- 2) Abbott, Ira H., and Doenhoff Abert E. Von. *Theory of Wing Sections: including a Summary of Airfoil Data*. Mineola: Dover Publications, 1999. Print. 452.
- 3) Abbott, Ira H., and Doenhoff Abert E. Von. *Theory of Wing Sections: including a Summary of Airfoil Data*. Mineola: Dover Publications, 1999. Print. 488.
- 4) Anderson, John David. *Introduction to Flight*. Boston: McGraw-Hill Higher Education, 2005. Print. 331.
- 5) Pope, Alan, and John J. Harper. *Low-speed Wind Tunnel Testing*. New York ; Toronto: J. Wiley, 1966. Print. 320.
- 6) Anderson, John David. *Introduction to Flight*. Boston: McGraw-Hill Higher Education, 2005. Print. 332.